Progress In Electromagnetics Research M, Vol. 67, 35–44, 2018

Gain and Noise Performance of Non-Foster Matching Circuit for VLF Receiver Loop Antenna

Yalong Yan, Chao Liu*, Yinghui Dong, and Huaning Wu

Abstract—Non-Foster matching circuits are those that can function as negative capacitors or inductors, and can thus overcome the gain-bandwidth limitation of passive matching circuits for antennas. This paper presents a non-Foster matching circuit (NFC) for a very low frequency (VLF) receiver loop antenna. The bandwidth of the antenna was improved by 383%, and the average gain was improved in most bands compared to a passive matching circuit (over 15–30 kHz). In contrast to circuits reported in other publications, the signal to noise ratio (SNR) of the passive matching network performed better than the non-Foster matching network. To analyze this phenomenon, a noise model was developed for the simplified balanced NFC, and noise analysis was conducted between the non-Foster and passive matching networks, which indicates that the non-Foster matching circuits cannot provide a better SNR performance than the passive matching circuits under low noise figure level receiver conditions.

1. INTRODUCTION

Non-Foster circuits can overcome the fundamental gain-bandwidth limitation as first described by Wheeler [1] and Chu [2], allowing for the development of applications in superluminal waveguides [3], broadband metamaterials [4], phase shifters [5] and antennas [6–8]. The non-Foster circuit can generate a "negative capacitor" or "negative inductor", thus to overcome the capacitance or inductance of the matching antenna. Fig. 1 shows how an ideal negative inductor can cancel a positive inductance over the bandwidth, as compared to the conventional passive matching method which can only cancel the inductance of the antenna at a single frequency.

Several NFC topologies have been reported to date [9–11], most of which were designed for enhanced stability and bandwidth performance. Different NFCs, including CMOS based NFC [12], diode based NFC [13] and amplifier based NFC [14], have been matched to various types of antennas, including the monopole antenna [15], loop antenna [16], Egyptian axe dipole antenna [17], microstrip leaky-wave antenna [18], and parasitic array [19], with mostly favorable results. The results show that the NFCs can truly enlarge the bandwidth of the antennas and maintain a stability condition at the same time.

As for the antenna's non-Foster matching circuits design frequency band, earlier researchers have concentrated on the high frequency (HF) band, but little is known about the antenna's operation frequency band enlargement process, especially below HF. VLF receiver loop antennas, which are common in submarines as a signal reception component, are a good example of this. As submarines usually receive signal under water, VLF which has a long wavelength is the main communication method for submarine communication as a result. The receiver antennas equipped on submarines are long wire antennas or loop antennas which have an inductive characteristic, the analysis focuses on the "negative inductor" design in VLF as a result. Also, most publications have concentrated on the gain and bandwidth performance of the NFC loaded antenna as the negative reactance slope; frequency provided by the NFC can compensate for the equivalent capacitance or inductance of the antenna, thus improving

Received 9 February 2018, Accepted 21 March 2018, Scheduled 5 April 2018
* Corresponding author: Chao Liu (liuchaonue@sina.com).
The authors are with the Department of Electronic Engineering, Naval University of Engineering, Wuhan 430033, China.

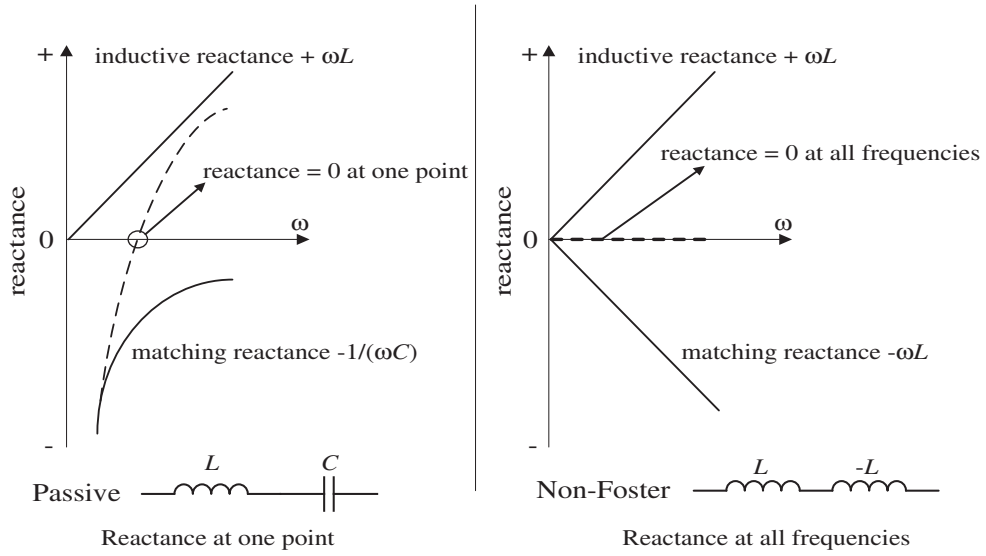

Figure 1. Passive versus non-Foster resonance of a positive inductor.

the gain and bandwidth of the antenna. However, the SNR of the antenna has to be considered as well. Very few publications have taken this into account [6, 8]. As the NFC is composed of active devices, the noise generated by these devices will contribute to the overall system noise and degrade the SNR of the antenna. Therefore, we focus on analyzing the SNR performance of the NFC for the VLF receiver loop antenna in this paper.

The paper is structured as follows. Section 2 presents the design process of the receiver loop antenna. The design topology of the NFC and the gain, bandwidth, noise and SNR results are presented in Section 3. Section 4 provides the noise model and simulated noise figures of the NFC and passive matching antenna. Section 5 provides a brief conclusion.

2. LOOP ANTENNA DESIGN PROCESS

The wire antenna used in submarine is too long (200 m) for laboratory design and test, so a loop antenna is selected as the VLF receiver antenna for the response that has a shield case that is 30 dB lower than the same effective height whip antenna at a 0.005 distance from the static noise source (100 m at the frequency of 15 kHz) [20].

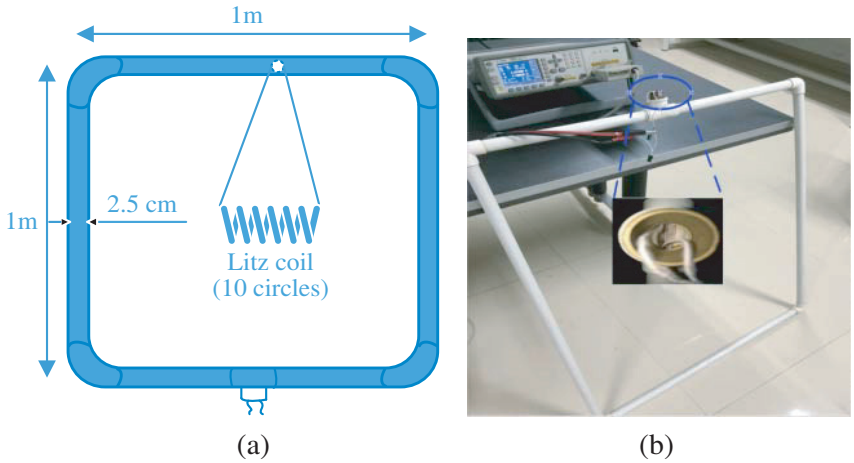

Figure 2. (a) Schematic diagram of rectangle loop antenna with shield case; (b) Photograph of rectangle loop antenna with shield case (valid at a single frequency).

The loop antenna was designed to use a litz wire to degrade the loss, thus improving the Q value and efficient height of the antenna. The litz wire (99 circles per string, 20 strings, 1980 circles in total) was circled inside a shield pipe, and the PVC pipe acts as a supporting function of the litz wire. A schematic diagram of the rectangle loop antenna is shown in Fig. 2(a). Fig. 2(b) shows a photograph of the antenna.

It is difficult to model the designed loop antenna in electromagnetism (EM) simulation software such as FEKO or HFSS, because the simulation time lasts too long for the 1980 circles of litz wire. Therefore, a vector network analyzer (VNA) was used to directly measure the input impedance characteristics of the antenna from 15 to 30 kHz. The measured S-parameters of the loop antenna are shown in Fig. 3, from which we can observe that the antenna has a low gain, and there are no self-resonance points over the entire bandwidth.

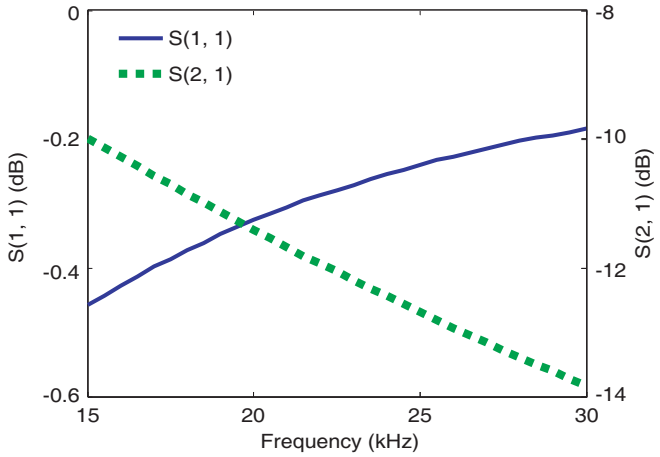

Figure 3. Measured S-parameter data of the VLF receiver loop antenna.

3. MATCHING OF LOOP ANTENNA WITH NFC

3.1. NFC and Passive Matching Networks Design

A floating open-circuit stable configuration of Linvill's NFC, which is shown in Fig. 4, was implemented with a low-noise NPN silicon bipolar transistor (NEC NE85630) on a standard 1.5 mm-thick PCB board; the antenna's S2P model in Fig. 3 was generated according to [21]. The circuit was optimized by a genetic algorithm to have low loss in the matching bandwidth, while providing a higher gain of the antenna. Two objective functions were set in the ADS optimize control unit, the first one is:

$$-20 < \text{abs}\left(\text{imag}(Z_{in1})\right) < 20 \tag{1}$$

The second one is:

$$-20 < \text{abs}\left(\text{real}(Z_{in1}) - 50\right) < 20 \tag{2}$$

With the introduction of the two objective functions above, the elements' values were reconfigured. The input resistance of the matching circuit can be closer to 50 Ω, and the input reactance can be closer to 0 Ω.

R_3 is used in the control of current mutation situations. L_1 is the load inductor, which can be transformed to a "negative inductor" by the NFC. Its value (0.77 mH) is larger than the equivalent inductor of the loop antenna (0.65 mH measured), which conforms with the stability requirement of the NFC [7]. Also, tuning the values of the elements after optimization could make the NFC obtain a better bandwidth and gain performance. During the tuning process, it is found that L_1 relates more closely to the S_{11} of the two-port matching network, which changes the S_{11} minimum value's corresponding frequency point. L_0 determines the magnitude of the minimum S_{11} value and maximum S_{21} value.

A "best effort" passive matching network (Fig. 5) with a resonance frequency of 22.5 kHz was designed for comparison with the non-Foster matching network. The values of the two capacitors in

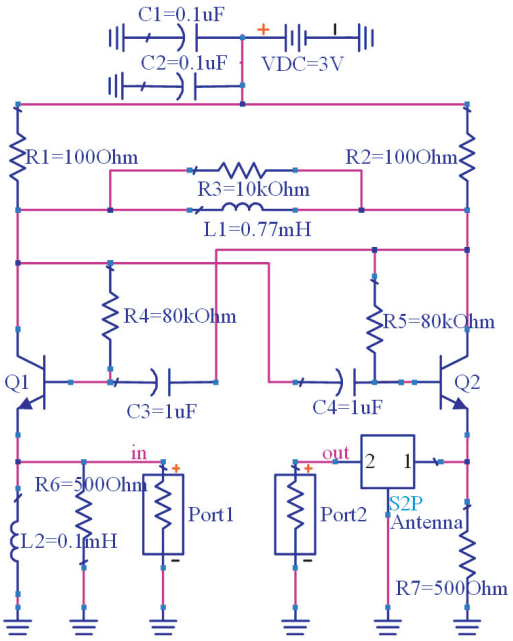

Figure 4. An open circuit stable balanced non-Foster matching network.

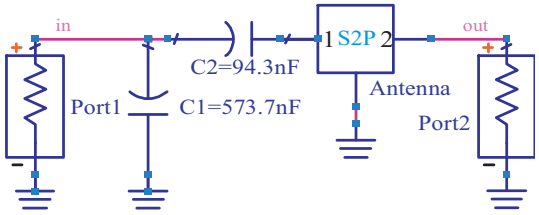

Figure 5. The designed passive matching network.

the passive matching circuit were also optimized by the genetic algorithm in ADS to make the network reach a lower S_{11} value and a higher S_{21} value.

3.2. Bandwidth and *S*-Parameters Measurements

To examine the reflection and transmission coefficients of the designed non-Foster matching network, following the measuring method in [6], the S_{11} and S_{21} measurements setups are shown in Fig. 6(a) and Fig. 6(b), respectively. When conducting the S_{21} measurement, the signal transmitted from the VNA was set to -5 dBm. The non-Foster and passive matching circuits were attached to the VNA to obtain the comparison results. The frequency of the transmitted signal was swept from 15 kHz to 30 kHz.

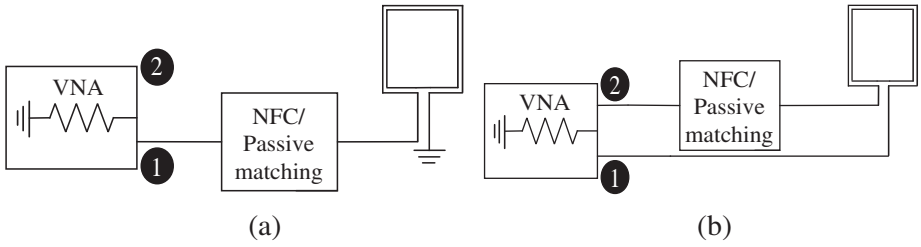

Figure 6. (a) S_{11} measurement diagram for non-Foster matched antenna and passive antenna; (b) S_{21} measurement diagram for non-Foster matched antenna and passive antenna (the passive matching and non-Foster matching circuits are attached to the antenna).

The simulated and measured results of S_{11} and S_{21} of the non-Foster and passive matching networks are shown in Fig. 6. It can be observed in Fig. 7 that the simulated results are similar to the measured ones, validating our *S*-parameters measurements. The result can be observed from Fig. 7(a) — the -10 dB S_{11} fractional bandwidth of the NFC loaded case is 18% from 15 kHz to 30 kHz, marking a 383% improve over the passive loaded antenna (4.7%). From Fig. 7(b) we can observe that although the S_{21} provided by the NFC matching network decreased by 25% maximum at the resonant point, it increased over 15–21.8 kHz and 23.1–30 kHz, thus the NFC-enhanced S_{21} is superior to the passive

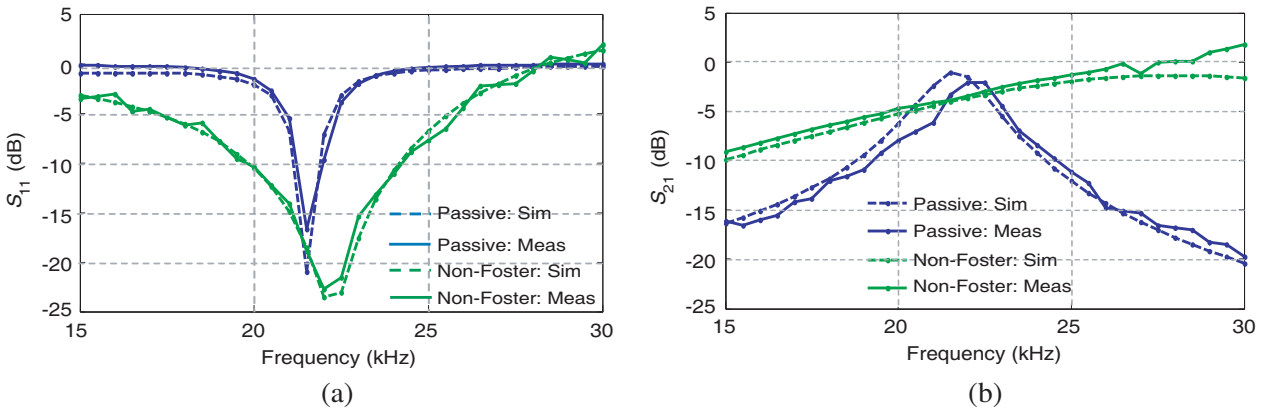

Figure 7. (a) Comparison of measured and simulated S_{11} of NFC and passive matching network; (b) Comparison of measured and simulated S_{21} of the NFC and passive matching network.

loaded case over most frequency bands in the VLF (15 kHz–30 kHz). Therefore, the NFC can provide a larger -10 dB S_{11} fractional bandwidth and higher S_{21} value compared with the passive matching circuit.

3.3. Noise and Antenna Gain Measurements

The antenna's SNR performance is the most important parameter in actual work. To access the SNR performance of the matched antenna, a spectrum analyzer was used to record the total noise of the NFC and the passive matching circuit. Since the spectrum analyzer has a noise figure of 23 dB, as calculated from its noise floor power level, a low noise preamplifier with a gain of 25 dB and a noise figure (NF) of 3 dB was attached between the receiver (VNA) and the NFC to obtain a low noise receiving system with an NF of 4 dB. The total noise received by the receiver can be divided into three parts: the environmental noise, the added noise from the NFC, and the receiver noise floor. The noise generated by the NFC cannot be isolated from the total measured noise, so it is not possible to calculate the noise figure of this system. However, combining the gain results obtained, the SNR improvement can be calculated based on the total noise measured by the spectrum analyzer. The noise and gain measurement setup is shown in Fig. 8. This measured noise power and the antenna gain of the NFC

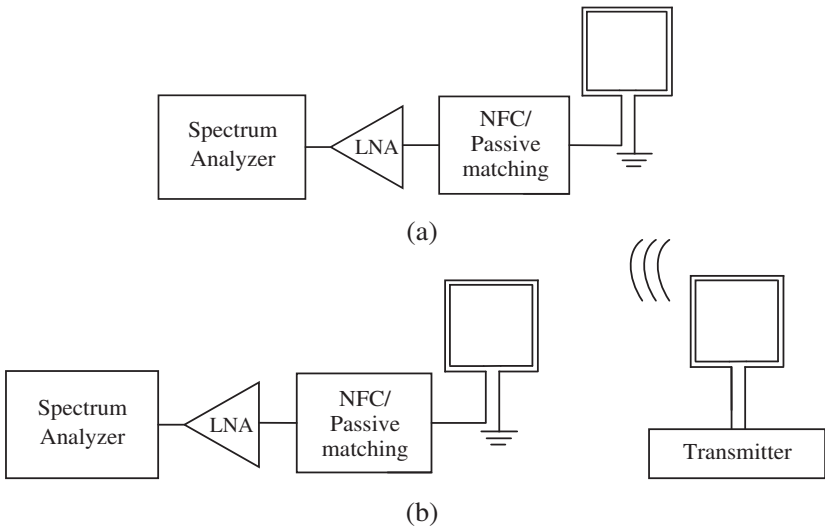

Figure 8. (a) Measurement setup to determine noise added by the NFC and passive matching circuit; (b) Measurement setup to determine gain provided by the NFC and passive matching circuits.

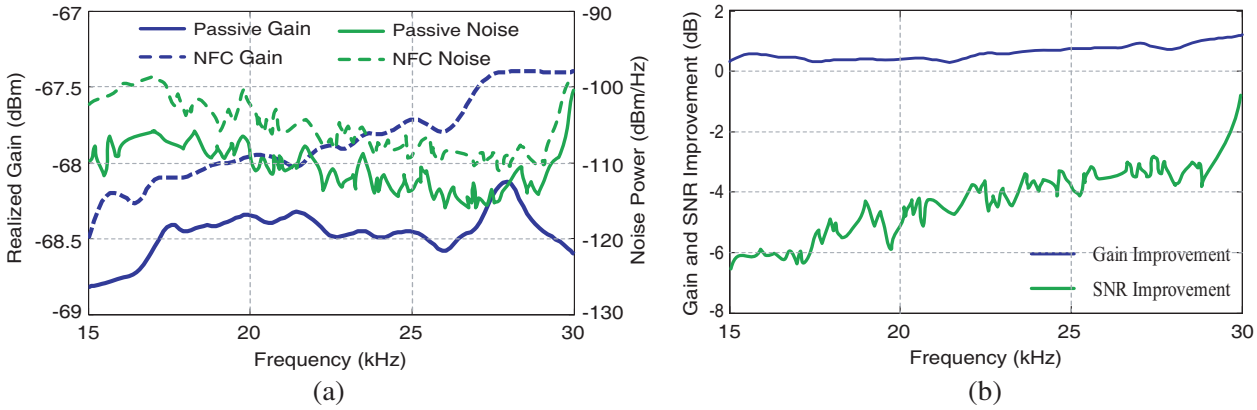

Figure 9. Measurement setup to record (a) gain, noise of passive and non-Foster matching networks; (b) gain, SNR improvement of passive and non-Foster matching networks.

network and passive matching network are shown in Fig. 9(a). Fig. 9(b) shows the SNR performance between the NFC and passive matching network.

It can be observed from Fig. 9(a) that the received signal gain provided by the NFC is higher than the passive matching case. The average gain improvement is calculated as 1.1 dB. The noise generated by the NFC matching network is also higher than the passive matching case. The SNR can be then calculated as

$$\mathrm{SNR}_{\mathrm{improvement}} = \mathrm{Gain}_{\mathrm{improvement}} - \mathrm{Noise}_{\mathrm{improvement}} = (S_1 - S_2) - (N_1 - N_2) \tag{3}$$

where S_1, S_2 are the measured signal level provided by the NFC and passive matching circuits, and N_1, N_2 are the measured system noise provided by the NFC and passive matching circuits. From Fig. 9(b) it can be observed that the non-Foster matching network cannot provide an actual SNR improvement over the passive matching network in the low noise receiving system, which does not meet the conclusions in [6]. Therefore, a thorough investigation of the gain and noise of the NFC and passive matching networks should be conducted to analysis this phenomenon.

4. NOISE ANALYSIS OF THE NFC AND PASSIVE MATCHING NETWORK

4.1. Matching Circuit Model Design

The last section shows that with a 4 dB noise figure receiver, the NFC network cannot provide an SNR improvement over the passive matching network. We then speculated that in the low noise receiving system, unlike the noise condition in [6], the noise generated by the NFC cannot be masked by the receiver's noise floor; in this situation, the NFC noise dominates, and thus the noise improved by the NFC is higher than the gain improved by the NFC; therefore, the SNR degrades compared with the passive matching circuit. To examine this assumption, a simplified open stable balanced Linvill Negative Impedance Convertor (NIC) and a passive matching circuit (Fig. 10) were proposed to examine their noise figures under the same receiving conditions.

In Fig. 10(a), the loop antenna was modeled with a reactance jX_{Loop} and a radiation resistance R_r with an antenna noise temperature T_{Loop}; the values of jX_{Loop} and R_r were measured by the VNA in Section 2. The antenna noise temperature T_{Loop} was modeled as man-made environmental noise in rural areas [22]. The NFC was modeled as a perfectly lossless reactance jX_{Loop}, along with an equivalent open circuit noise voltage $\overline{v_{\mathrm{NIC}}}$. The NF of the NIC and passive matching circuits can be expressed in decibels (dB) as

$$NF = 10\log\left(1 + \frac{N_{\mathrm{NIC/PASSIVE}} + N_{\mathrm{RX_{NIC/PASSIVE}}}}{N_{in} \cdot \mathrm{Gain}_{\mathrm{NIC/PASSIVE}}}\right) \tag{4}$$

where N_{NIC} is the noise power of the NIC, and $N_{\mathrm{RX_{NIC}}}$ is the internal noise power retained at the receiver. N_{in} is the input noise power, which is given by kT_{Loop}. The output noise value of the passive

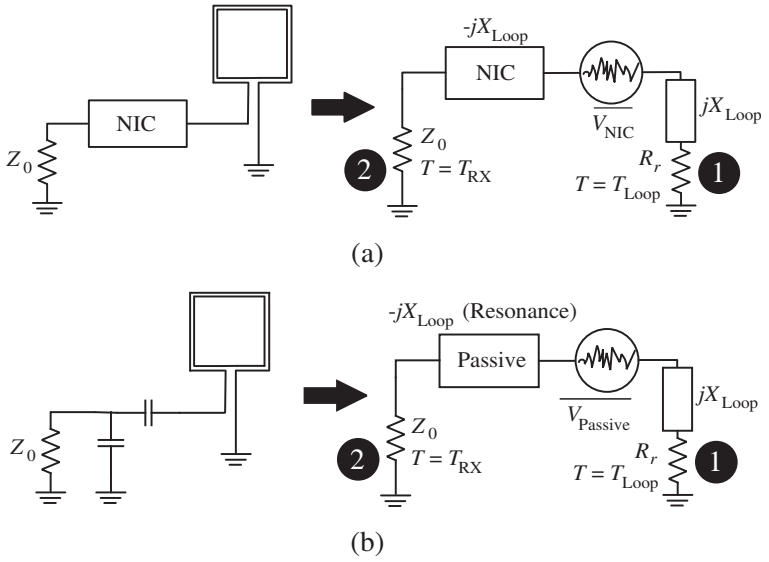

Figure 10. (a) NIC attached to the loop antenna and a noise receiver; (b) Passive matching circuit attached to the loop antenna and a noise receiver.

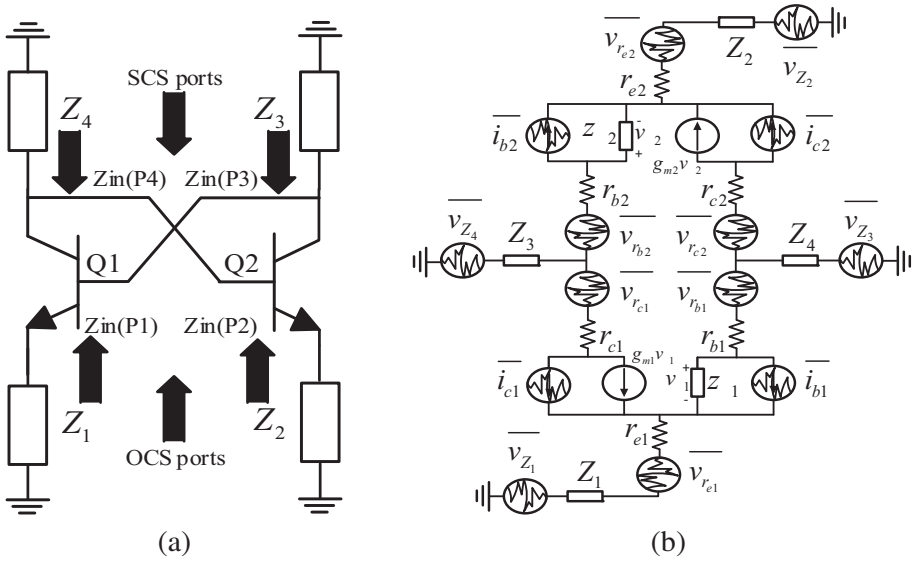

Figure 11. (a) Topology of an NIC; (b) Representation of voltage and current noise sources in a general NIC.

matching circuit was derived in [23], so the model of the NIC will be focused on next.

The general topology of the NIC is shown in Fig. 11(a), and its extended topology is shown in Fig. 11(b) (the small model of the two transistors along with the noise sources of the transistors). In Fig. 11(a), the balanced open circuit stable (OCS) input impedance is seen by looking at ports Z_1 and Z_2, and the balanced short circuit stable (SCS) input impedance is seen by looking at ports Z_3 and Z_4.

We focus on the balanced OCS NIC model design process shown in Fig. 4; this is the kind of NIC we proposed. In this situation, the thermal noise voltage $\overline{v_{r_b}}$, $\overline{v_{r_c}}$, $\overline{v_{r_e}}$, $\overline{v_{z_1}}$, $\overline{v_{z_2}}$, $\overline{v_{z_3}}$ and v_{z_4} represent the thermal noise voltage of the base resistor, the collector resistor, the emitter resistor and the real part of the attached loads Z_1, Z_2, Z_3, Z_4. The noise voltages are considered as $\sqrt{4kTR}$, and the shot noise currents of the collector current and base current are

$$\overline{i_c} = \sqrt{2qI_c} \tag{5}$$

$$\overline{i_b} = \sqrt{2q\frac{I_c}{\beta}} \tag{6}$$

where I_c is the bias current of the collector, and β is the gain I_c/I_b of the current.

The circuit model shown in Fig. 11(b) is used to derive the equivalent open circuit noise voltage $\overline{v_{\text{NIC}}}$ for the OCS NIC. The equivalent noise transformations are shown below.

$$Z_{\text{in}_B} \approx r_{e1} + r_{e2} + \frac{1}{g_{m1}} + \frac{1}{g_{m2}} - Z_{\text{load}} - R_{\text{load}} \tag{7}$$

$$\overline{v_{i_{c,eq}}} = \left|\overline{i_c} \times \left[\frac{Z_{\text{load}}}{2} + \frac{Z_{\text{in}_B}}{2} - r_e + \frac{R_{\text{load}}}{2}\right]\right| \tag{8}$$

$$\overline{v_{i_{b,eq}}} = \left|\overline{i_b} \times \left[\frac{Z_{\text{load}}}{2} - \frac{Z_{in_B}}{2} + r_e + r_b + \frac{R_{\text{load}}}{2}\right]\right| \tag{9}$$

where $\overline{i_c} = \sqrt{2qI_c}$ and $\overline{i_b} = \sqrt{2q\frac{I_c}{\beta}}$.

$$\overline{v_{r_{e,eq}}} = \sqrt{4kTr_e} \tag{10}$$

$$\overline{v_{r_{b,eq}}} = \sqrt{4kTr_b} \tag{11}$$

$$\overline{v_{R_{\text{load},eq}}} = \sqrt{4kTR_{\text{load}}} \tag{12}$$

$$\overline{v_{\text{NIC}_B}} = \sqrt{2\left|\overline{v_{i_{c,eq}}}\right|^2 + 2\left|\overline{v_{i_{b,eq}}}\right|^2 + 2\left|\overline{v_{r_{e,eq}}}\right|^2 + 2\left|\overline{v_{r_{b,eq}}}\right|^2 + \left|\overline{v_{R_{\text{load},eq}}}\right|^2} \tag{13}$$

An interesting result is that when assuming a very large transconductance g_m, and a near-zero emitter and base resistance (ideal situation), Equations (8), (10), (11), (12) equal 0, and the total equivalent voltage noise $\overline{v_{\text{NIC}_B}}$ is calculated as $|i_b \times Z_{\text{load}}|$, which is proportional to the impedance of the NIC (Equation (7)). Based on this corollary, the voltage noise can be calculated in a much easier way.

To examine the noise model we proposed, the simulation for a simplified model of the NIC (Fig. 11(a)) was done in Keysight ADS for comparison with the calculated noise voltage using the equations above. The results are shown in Fig. 12. From Fig. 12, it can be observed that the simulated results match well with the calculated results; thus, the noise model proposed can be verified. After verifying the noise model designed, the noise figure of the non-Foster matching and passive matching networks can be proceeded.

4.2. Noise Figure of the Non-Foster and Passive Matching Networks

The noise figure in (2) can be further expanded as shown below.

$$N_{\text{NIC}} = \left|\overline{v_{\text{NIC}}} \times \frac{Z_0}{Z_0 + Z_{in_{\text{NIC}}} + Z_{\text{Loop}}}\right|^2 \times \frac{1}{Z_0} \tag{14}$$

$$N_{\text{PASSIVE}} = \left|\overline{v_{\text{PASSIVE}}} \times \frac{Z_0}{Z_0 + Z_{\text{out}_{\text{PASSIVE}}}}\right|^2 \times \frac{1}{Z_0} \tag{15}$$

$$N_{\text{RX}_{\text{NIC}}} = \left|2\sqrt{kT_{\text{RX}}Z_0} \cdot \frac{Z_{in_{\text{NIC}}} + Z_{\text{Loop}}}{Z_0 + Z_{in_{\text{NIC}}} + Z_{\text{Loop}}}\right|^2 \times \frac{1}{Z_0} \tag{16}$$

$$N_{\text{RX}_{\text{PASSIVE}}} = \left|2\sqrt{kT_{\text{RX}}Z_0} \cdot \frac{Z_{\text{out}_{\text{PASSIVE}}}}{Z_0 + Z_{\text{out}_{\text{PASSIVE}}}}\right|^2 \times \frac{1}{Z_0} \tag{17}$$

$$N_{in} \cdot \text{Gain}_{\text{NIC/PASSIVE}} = kT_{\text{Loop}} \times \left|S_{21_{\text{NIC/PASSIVE}}}\right|^2 \tag{18}$$

where N_{NIC} and N_{PASSIVE} are the noise from the NIC and passive matching circuit, respectively; $Z_{\text{in}_{\text{NIC}}}$ and Z_{Loop} are the input impedance of the NIC and the loop antenna, respectively; $Z_{\text{out}_{\text{PASSIVE}}}$ is the impedance seen looking from the receiver into the output of the amplifier in Fig. 10(b); and T_{RX} and

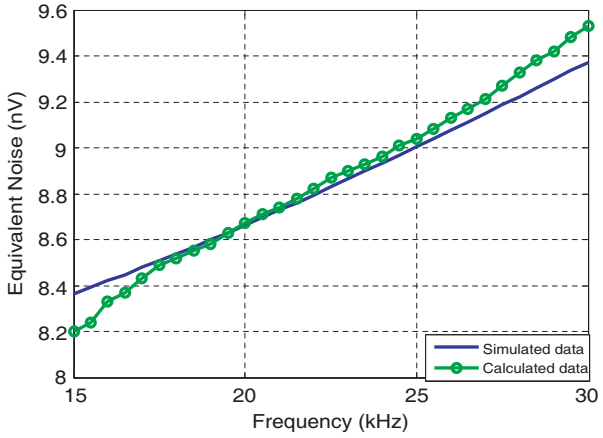

Figure 12. Simulated and calculated total equivalent noise for a balanced OCS negative inductor.

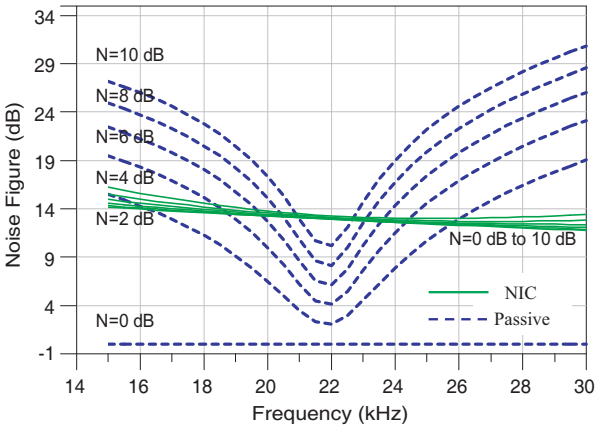

Figure 13. Noise figure comparison between the non-Foster and passive matching networks for different noisy receivers (N represents the noise figure of the receiver N_{RX}).

T_{Loop} are the noise temperatures of the receiver and the antenna, respectively. The calculation method of these parameters have all been given in the previous sections.

Then, the noise figures of the non-Foster and passive matching networks were simulated. In both matching networks, the noise figure of the receiver was swept from 0 dB (ideal noiseless receiver) to 10 dB (step size 2 dB), and the simulated results are shown in Fig. 13. It is observed that the noise figure of the non-Foster matching network is largely independent of the swept receiver noise levels. This is because the internal noise of the receiver is radiated back out through the antenna in the non-Foster system, leading to a receiver noise level $N_{\mathrm{RX_{NIC}}}$ in Equation (4) that is 20 dB less than the noise level $N_{\mathrm{RX_{PASSIVE}}}$ of the passive matching network, as verified by Equation (16) and (17). Therefore, the effect of N_{RX} in Equation (4) can be neglected for the non-Foster matching network.

From the simulated results, we can thus see that under the same input SNR conditions, the passive matching network provides a better SNR performance than the non-Foster matching case with a noise figure receiver below 4 dB over most bands. With the increase of the receiver's noise figure, the non-Foster matching case gradually provides a better SNR performance than the passive matching case. Note that near the resonance point, the passive matching case always provides a received SNR advantage compared to the non-Foster matching case.

5. CONCLUSION

This paper presents the bandwidth, gain and SNR performance of a non-Foster matching network in VLF. The simulated and measured results show that the non-Foster matching network can provide a larger bandwidth and higher gain than the passive matching case, but with disadvantageous performance on the SNR. To examine this point, a noise model of the NIC was proposed, and the noise figure of the non-Foster and passive matching networks under different noisy receiver conditions was simulated. It is found that in the low noise figure receiver condition (below 4 dB), the non-Foster matching network cannot provide a better SNR performance than the passive matching network, because the noise generated by the NIC cannot get masked by the receiver's noise floor; thus, the overall system noise figure is affected. Therefore, the non-Foster matching network cannot provide an actual better SNR performance than the passive matching network in a low noise receiver system (NF$<$4 dB).

REFERENCES

1. Wheeler, H. A., "Fundamental limitations of small antennas," *Proceedings of the IRE*, Vol. 35, No. 12, 1479–1484, Dec. 1947.

2. Chu, L. J., "Physical limitations of omni-directional antennas," *Journal of Applied Physics*, Vol. 19, No. 12, 1163-1175-729, Jun. 1948.
3. Long, J., M. M. Jacob, and F. S. Daniel, "Broadband fast-wave propagation in a non-Foster circuit loaded waveguide," *IEEE Trans. Antennas Propag.*, Vol. 62, No. 4, 789–798, Apr. 2014.
4. Saadat, S., M. Adnan, H. Mosallaei, et al., "Composite metamaterial and metasuiface integrated with non-Foster active circuit elements: A bandwidth-enhancement investigation," *IEEE Trans. Antennas Propag.*, Vol. 61, No. 3, 1210–1218, Mar. 2013
5. Gao, F., F. S. Zhang, J. Long, et al., "Non-dispersive tunable reflection phase shifter based on non-Foster circuits", *Electronics Letters*, Vol. 50, No. 22, 1616–1618, Oct. 2014
6. Sussman-Fort, S. E. and R. M. Rudish, "Non-Foster impedance matching of electrically-small antennas," *IEEE Trans. Antennas Propag.*, Vol. 57, No. 8, 2230–2241, Aug. 2009
7. White, C. R. and J. S. Colburn, "A non-Foster VHF monopole antenna," *IEEE Antennas and Wireless Propag. Lett.*, Vol. 11, No. 4, 584–587, Jun. 2012.
8. Jacob, M. M. and D. F. Sievenpiper, "Gain and noise analysis of non-Foster matched antennas," *IEEE Trans. Antennas Propag.*, Vol. 64, No. 12, 4993–5004, Jun. 2016.
9. Obeidat, K. A., B. D. Raines, and R. G. Rojas, "Application of characteristic modes and non-Foster multiport loading to the design of broadband antennas," *IEEE Trans. Antennas Propag.*, Vol. 58, No. 1, 203–207, Jan. 2010.
10. Debogovie, T., S. Hrabar, and J. Perruisseau-Carrier, "Broadband Fabry-Perot radiation based on non-Foster cavity boundary," *Electronics Letters*, Vol. 49, No. 4, 445–446, Feb. 2013.
11. White, C. R., J. W. May, and J. S. Colburn, "A variable negative-inductance integrated circuit at UHF frequencies," *IEEE Microw. Wireless Compon. Lett.*, Vol. 22, No. 1, 35–37, Jan. 2012.
12. Niang, A., A. de Lustrac, and S. N. Burokur, "Superluminal wave propagation in a non-Foster negative capacitor loaded transmission line," *Electronics Letters*, Vol. 53, No. 8, 547–549, Apr. 2017.
13. Nagarkoti, D. S., Y. Hao, et al., "Design of broadband non-Foster circuits based on resonant tunneling diodes," *IEEE Antennas and Wireless Propag. Lett.*, Vol. 15, 1398–1401, Apr. 2016.
14. Yang, H., I. Kim, and K. Kim, "Non-Foster matching of a resistively loaded vee dipole antenna using operational amplifiers," *IEEE Trans. Antennas Propag.*, Vol. 64, No. 4, 1477–1482, Apr. 2016.
15. Mirzaei, H. and G. Eleftheriades, "A resonant printed monopole antenna with an embedded non-Foster matching network," *IEEE Trans. Antennas Propag.*, Vol. 61, No. 11, 5363–5371, Aug. 2013.
16. Jacob, M. M., J. Long, and D. F. Sievenpiper, "Broadband non-Foster matching of an electrically small loop antenna," *Proceedings of the 2012 IEEE International Symposium on Antennas and Propagation*, 1–2, Jul. 2012.
17. Tang, M. C., N. Zhu, and R. W. Ziolkowski, "Augmenting a modified egyptian axe dipole antenna with non-Foster elements to enlarge its directivity bandwidth," *IEEE Antennas and Wireless Propag. Lett.*, Vol. 12, 421–424, Mar. 2013.
18. Muha, D., S. Hrabar, I. Krois, and I. Bonic, "Design of microstrip non-foster leaky-wave antenna," *Applied Electromagnetics and Communications (ICECom)*, 1–3, 2013.
19. Jacob, M. M., J. Long, and D. F. Sievenpiper, "Non-Foster loaded parasitic array for broadband steerable patterns," *IEEE Trans. Antennas Propag.*, Vol. 62, No. 12, 6081–6090, Oct. 2014.
20. Chao, L., *VLF Communications*, 99–100, Tide Press, Beijing, 2008.
21. Aberle, J. T., "Two-port representation of an antenna with application to non-Foster matching networks," *IEEE Trans. Antennas Propag.*, Vol. 56, No. 6, 1218–1222, May 2008.
22. Sailors, D., "Techniques for estimating the effects of man-made radio noise on distributed military systems," *In AGARD, Use or Reduction of Propagation and Noise Effects in Distributed Military Systems, Conference Proceedings*, Vol. 1, 14, SEE N91-30362 22-32, 1990.
23. Andrews, C. and A. Molnar, "Implications of passive mixer transparency for impedance matching and noise figure in passive mixer-first receivers," *IEEE Trans. Antennas Circuits and Systems.*, Vol. 57, No. 12, 3092–3013, Dec. 2010.